

Received 2024 December 10; accepted 2025 January 13

Spectroscopic study of the late B-type eclipsing binary system AR Aurigae A and B: Towards clarifying the differences in atmospheric parameters and chemical abundances

Yoichi Takeda

11-2 Enomachi, Naka-ku, Hiroshima-shi, 730-0851, Japan; ytakeda@js2.so-net.ne.jp

Abstract AR Aur A+B is a close binary of astrophysical interest, because dissimilar surface compositions are reported between similar late B-type dwarfs. A new spectroscopic study on this system was carried out based on the disentangled spectra, in order to determine their atmospheric parameters and elemental abundances. The effective temperature and microturbulence (determined from the equivalent widths of Fe II lines) turned out (11150 K, 0.9 km s^{-1}) and (10650 K, 0.1 km s^{-1}) for A and B. The chemical abundances of 28 elements were then derived while taking into account the non-LTE effect for $Z \leq 15$ elements (Z : atomic number). The following trends were elucidated for $[X/H]$ (abundance of X relative to the Sun): (1) Qualitatively, $[X/H]$ shows a rough global tendency of increasing with Z , with the gradient steeper for A than for B. (2) However, considerable dispersion is involved for A, since prominently large peculiarities are seen in specific elements reflecting the characteristics of HgMn stars (e.g., very deficient N, Al, Sc, Ni; markedly overabundant P, Mn). (3) In contrast, the Z -dependence of $[X/H]$ for B tends to be nearly linear with only a small dispersion. These observational facts may serve as a key to understanding the critical condition for the emergence of chemical anomaly.

Key words: stars: abundances – stars: atmospheres – stars: binaries: spectroscopic – stars: chemically peculiar – stars: early-type – stars: individual (AR Aur)

1 INTRODUCTION

AR Aur is an eclipsing double-line spectroscopic binary ($P = 4.135$ d) consisting of late B-type stars (B9 + B9.5; hereinafter the former/latter primary/secondary components are denoted as A/B, respectively). An especially interesting aspect of astrophysical interest regarding this system is that the chemical abundances of both components are different despite of their apparent similarity. That is, the slightly hotter A exhibits a chemically peculiar feature of HgMn type (e.g., detection of Hg II 3984 line) while the other B does not. This distinction in the surface chemistry between near-identical component stars (which should have born with the same composition) was recognized already a half century ago (Wolff & Wolff 1976; Takeda et al. 1979; see also sect. 2 in Khokhlova et al. 1995). Therefore, this binary system can be an important testing bench for clarifying the condition for the advent of chemical anomaly. To that end, the atmospheric parameters and the elemental abundances for both components should be known to a sufficient precision.

Yet, due to the difficulty of measuring individual lines in the spectrum (because those of A and B intricately co-exist and merge), only a few abundance determinations of AR Aur A and B have been published so far:

- Khokhlova et al. (1995) carefully measured the equivalent widths of A and B from the double-line spectra in 3850–4600 Å and determined the abundances of 18 elements for both components by using the curve-of-growth method.
- Based on the equivalent width data published by Khokhlova et al. (1995), Ryabchikova (1998) redetermined the abundances of AR Aur A and B (along with other HgMn binary stars) by way of the model atmosphere analysis.
- Zverko et al. (1997) applied the disentangling technique to obtain the individual spectra of A and B in 3910–4630 Å, and derived the abundances of 7 elements for both components by means of spectrum synthesis.
- The most extensive and notable work on the chemical abundances of AR Aur A and B is that of Folsom et al. (2010). They employed the spectrum-disentangling method to get the separated spectra of A and B (4170–6200 Å),

from which the abundances of ~ 30 elements were derived by using the spectrum-synthesis method.

- Similarly, based on the numerically disentangled spectra of AR Aur A and B (along with other four A-type spectroscopic binaries), Takeda et al. (2019; hereinafter referred to as Paper I) determined the abundances of 9 elements (though the primary attention was paid only to CNO) by applying the synthetic spectrum-fitting method.

These previous studies arrived at almost the similar conclusion of distinct HgMn-type abundance anomaly in A while a kind of less pronounced weak peculiarity in B. But some concern still remains regarding the choice of atmospheric parameters.

A potentially important issue is the choice of effective temperature (T_{eff}), which may be one of the critical parameters responsible for the onset of chemical anomaly. All of the previous investigations mentioned above adopted T_{eff} values of 10950 K (A)¹ and 10350 K (B), which are the spectrophotometric values (with an uncertainty of ± 300 K) determined by Nordström & Johansen (1994; see sect. 5 therein) by comparing the observed spectral energy distribution (SED) of AR Aur (3300–7850 Å) with the calculated model flux (A+B combined). Folsom et al. (2010) independently tried this SED-fitting method and obtained 10950 ± 150 K (A) and 10350 ± 150 K (B); i.e., the same results as derived by Nordström & Johansen (1994) even with smaller errors. It may as well be questioned, however, whether T_{eff} 's of two similar stars (especially their difference) are sufficiently well determinable based on the apparent SED of AR Aur (combined SEDs of both components) alone. Therefore, in order to check these results, it would be worthwhile to apply the alternative spectroscopic approach, in which T_{eff} is determined by requiring the consistency of abundances derived from many lines of various lower excitation potential (χ_{low}).

Another parameter of concern is the microturbulence (v_t), which more or less affects abundance determinations, especially when stronger lines are concerned. As a matter of fact, none of the above-mentioned past investigations could

¹ In Khokhlova et al.'s (1995) table 4 is given $T_{\text{eff}} = 10900$ K for AR Aur A, although $T_{\text{eff}} = 10950$ K is listed in their table 1. The reason for this slight difference is not clear.

successfully determine this parameter. Khokhlova et al. (1995) could estimate only the upper limit of $v_t < 1.0 \text{ km s}^{-1}$ for both A and B, and thus a value of 0.5 km s^{-1} was tentatively assumed in their analysis. The same treatment was adopted also by Ryabchikova (1998) and Zverko et al. (1997). Quite similarly, Folsom et al. (2010) could derive only the upper limit of 1 km s^{-1} for A and B, and they eventually employed $v_t = 0 \text{ km s}^{-1}$ for both components in their analysis. In the author's abundance determination in Paper I, 1.0 km s^{-1} (A) and 1.6 km s^{-1} (B) were tentatively assumed by roughly extrapolating the analytical T_{eff} -dependent relation empirically derived by Takeda et al. (2008) for A-type dwarfs ($7000 \lesssim T_{\text{eff}} \lesssim 10000 \text{ K}$). Accordingly, given that microturbulence of AR Aur has never been reliably determined so far, it is desirable to establish this parameter by the conventional method using many lines (e.g., Fe lines) by requiring that abundances do not show any systematic dependence upon equivalent widths.

Motivated by this situation, the author decided to conduct a new extensive spectroscopic analysis specific to AR Aur A and B based on the disentangled spectra of both components such as done in Paper I; but this time as much available spectral data as possible are exploited in order to make use of as many lines as possible.

Thus, the objectives and intended goals of this study are as follows.

- The spectrum-disentangling technique is applied to a set of spectra at various phases, in order to obtain disentangled spectra for A and B covering wide wavelength ranges (from violet to near-IR region) used for the analysis.
- Then, identification is done for as many spectral lines as possible, which are of good quality and judged to be usable abundance indicators, and their equivalent widths (W_λ) are measured.
- By using these W_λ of many Fe I and Fe II lines, T_{eff} and v_t are spectroscopically determined by requiring the condition of minimum abundance dispersion (i.e., absence of systematic dependence upon these parameters).
- Given such established atmospheric parameters, chemical abundances of various elements for both A and B are determined based on the W_λ data of identified lines, in order to ex-

amine the characteristics of surface chemistry and their differences between A and B.

- In addition, the spectrum-fitting approach is subsidiarily employed if necessary (e.g., for the cases of blended lines), and the non-LTE effect is taken into account wherever possible.

2 OBSERVATIONAL DATA

2.1 Spectrum disentangling

As in Paper I, the basic observational materials employed in this study are the high-dispersion spectra of AR Aur covering wide wavelength ranges ($\sim 3800\text{--}9200 \text{ \AA}$), which were obtained on 2010 December 14, 15, 16, 18, and 20 by using BOES (Bohyunsan Observatory Echelle Spectrograph) attached to the 1.8 m reflector at Bohyunsan Optical Astronomy Observatory (cf. sect. 2.1 and table 2 of Paper I for more details).

Then, the separated spectra of A and B were numerically obtained by applying the spectrum-disentangling technique to this set of original double-line (A+B) spectra at 11 different phases. For this purpose, the public-domain program CRES² written by Dr. S. Ilijić was employed with the same procedure as detailed in sect. 2.2 of Paper I. Yet, since this study intended to make use of spectra of wide wavelength region as available as possible, in contrast to the case of Paper I (where only selected 4 narrow regions were relevant), some specific considerations had to be made in preconditioning the original spectra to be disentangled.

- The existence of very strong lines with broad wings (such as H lines of Balmer or Paschen series) makes the disentangling process complicated. In order to circumvent this problem, the continuum normalization of all original spectra was done by regarding these wings of strong lines as if being the pseudo-continuum level, so that these features may be conveniently wiped out in the spectra. However, since this procedure does not work well in/near the sharply changing core regions of such lines, they had to be abandoned.
- Another problem of nuisance is the existence of telluric lines, which are appreciably seen in specific spectral regions (especially in longer wavelength ranges). These telluric features in

² <http://sail.zpf.fer.hr/cres/>

the original spectra were either removed in advance by dividing them by the spectrum of a rapid rotator or erased interactively by hand on the screen (if they are weak and not so many). However, those regions being dominated by very strong and numerous telluric lines had to be discarded, since their adequate removal turned out practically impossible.

In consequence, disentangled spectra of AR Aur A and B in 69 spectral regions (partially overlapped with each other) were obtained, which cover from $\sim 3900 \text{ \AA}$ to $\sim 9200 \text{ \AA}$ with a step of $\sim 0.05\text{--}0.1 \text{ \AA}$. The resulting spectra are graphically displayed in Figure 1a and 1b, where strong H lines are not seen any more and narrow spectral gaps (abandoned regions) are observed here and there. Likewise, how the signal-to-noise ratio (typically $\sim 200\text{--}600$) depend upon the wavelength is also shown in Figure 1c and 1d, where we can see that a maximum is attained around $\sim 6000 \text{ \AA}$. All these spectra used for the analysis are included in the online materials (“spectra_A.txt” and “spectra_B.txt”).

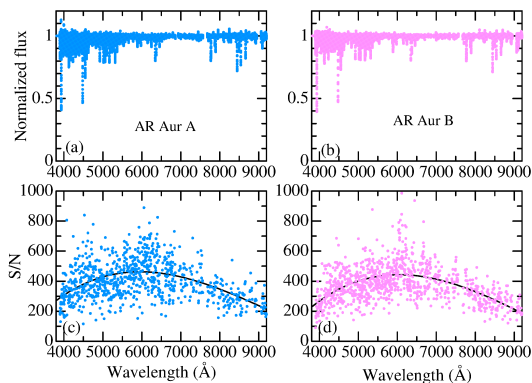


Fig. 1: The whole disentangled spectra of AR Aur A and B used in this study are plotted against wavelength in the upper panels (a) and (b). The runs of signal-to-noise ratios of these spectra (directly estimated in the line-free regions) are shown in the lower panels (c) and (d), where the fitted 3rd-order polynomials (describing the global trends) are also depicted by solid lines.

2.2 Line identification and equivalent widths

Based on the disentangled spectra, lines usable for abundance determinations were identified and their equivalent widths were measured. The identification was done by carefully comparing the observed spectrum with the theoretically synthesized one. Here, lines to be measured were restricted to only those of single component (i.e., multiplet lines with fine structure such as Mg II 4481 were discarded), and those being seriously affected by blending with other neighborhood lines were avoided.

Since spectral line shapes of AR Aur are rather rounded (reflecting the projected rotational velocity of $v_i \sin i \simeq 23 \text{ km s}^{-1}$; cf. table 1 of Paper I), the equivalent width (W_λ) of each line was evaluated by fitting its profile with a specifically devised function, which was constructed by convolving the rotational broadening function with the Gaussian function in an appropriately adjusted proportion. Figure 2 displays the actual examples of how the equivalent widths were measured by function-fitting for selected 24 lines of different elements. All the data (W_λ along with the atomic data taken from VALD database; cf. Ryabchikova et al. 2015) of finally identified 606/538 lines for A/B are also presented as the online material (“identlist_A.dat” and “identlist_B.dat”).

3 ATMOSPHERIC PARAMETERS

3.1 Determination method

As mentioned in Section 1, one of the main objectives of this study is to establish T_{eff} and v_t for both AR Aur A and B by making use of many Fe lines (which are most numerous available). According to the traditional approach, T_{eff} can be determined by the requirement that the abundances (A_i) derived from the equivalent widths (W_i) of each line i ($i = 1, 2, \dots, N$; where N is the number of lines) do not systematically depend upon the lower excitation potential (χ_{low}) [excitation equilibrium], while v_t is determinable by demanding that A_i 's do not show any systematic trend irrespective of the strengths of lines (W_i) [curve-of-growth matching]. The desired solution (T_{eff}^*, v_t^*) simultaneously satisfying these two conditions can be obtained by finding the minimum of $\sigma(T_{\text{eff}}, v_t)$, where σ is the standard deviation of the abundances around the mean ($\langle A \rangle$) calculated for various combinations of (T_{eff}, v_t).

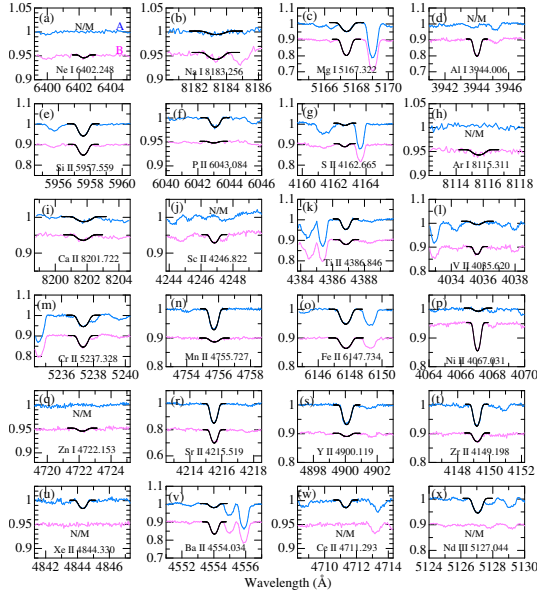


Fig. 2: In order to demonstrate how the equivalent widths were measured by applying the direct function-fitting method to those spectral lines identified and judged to be usable, selected cases of 24 lines (as indicated in each panel) are shown here. The observed spectra are shown in color (blue for A, pink for B), while the fitted function is depicted by black solid lines. Note that the scale marked in the ordinate is for A, since the spectra for B are shifted downwards by appropriate amounts (0.05 or 0.1 or 0.2). The cases where the line is too weak to be detected are indicated as “N/M”(Not Measurable).

The numbers of Fe I and Fe II lines (N_1 , N_2) among the list of identified lines (cf. Sect. 2.2) are (64, 306) for A and (90, 245) for B. For each species and each star, Fe abundances (A_i , $i = 1, 2, \dots, N$) were calculated from the equivalent widths (W_i , $i = 1, 2, \dots, N$) for an extensive grid of 1071 ($=51 \times 21$) cases resulting from combinations of 51 T_{eff} (from 9500 to 12000 K with a step of 50 K) and 21 v_t (from 0.0 to 2.0 km s^{-1} with a step of 0.1 km s^{-1}), where the necessary model atmospheres (solar metallicity models with $\log g = 4.3$)³ were generated by interpolating Kurucz’s (1993) grid of ATLAS9 models. Then,

³ Throughout this study, $\log g = 4.3$ is adopted for the surface gravity of both A and B, and solar metallicity models are used (cf. Sect. 3.2).

$\langle A \rangle$ and σ are calculated from the resulting set of (A_i , $i = 1, 2, \dots, N$) for each of the 1071 combinations of (T_{eff} , v_t), while outlier data (judged by Chauvenet’s criterion) were discarded.

The contour maps of such obtained σ_{1A} , σ_{2A} , σ_{1B} , and σ_{2B} on the $T_{\text{eff}}-v_t$ plane are depicted in Figure 3a, b, c, and d, respectively. The solutions of (T_{eff}^* , v_t^*) at the minimum of σ (denoted by crosses in Fig. 3) for each case are summarized in Table 1.

The resulting ($T_{\text{eff}}^*/v_t^*/\langle A \rangle$) derived from Fe I and Fe II lines are read from Table 1 as (10950/1.2/7.89)_{1A} and (11150/0.9/8.09)_{2A} for A, while (9900/0.0/7.30)_{1B} and (10650/0.1/7.79)_{2B} for B, where the values are rounded in consideration of the uncertainties. Therefore, while two kinds of results from Fe I and Fe II lines are not much different from each other for A, marked discordance is observed for the case of B in the sense that T_{eff} and $\langle A \rangle$ from Fe I (9900 K, 7.30) are considerably lower than that from Fe II (10650 K, 7.79).

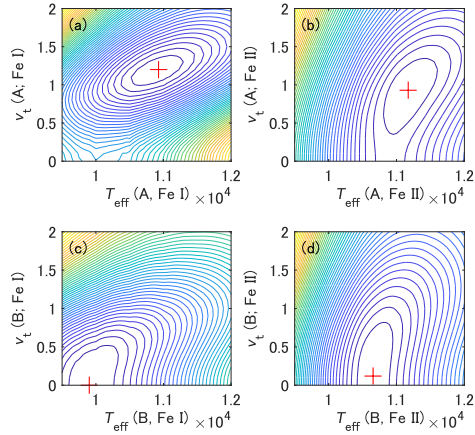


Fig. 3: Graphical display of the contours of $\sigma(T_{\text{eff}}, v_t)$, where the position of ($T_{\text{eff}}^{\text{min}}$, v_t^{min}) corresponding the minimum of σ is indicated by a cross. The upper panels (a, b) are for AR Aur A, while the lower ones (c, d) are for AR Aur B. The left panels (a, c) and the right ones (b, d) are for Fe I and Fe II, respectively.

3.2 Adopted parameters

Although two kinds of $(T_{\text{eff}}^*, v_t^*)$ solutions were derived in Section 3.1 from Fe I and Fe II lines, the latter Fe II results are considered to be more reliable than the former Fe I ones for several reasons: (i) Since only an extremely tiny fraction of Fe atoms remain neutral in the atmosphere of late B-type stars, the formation of Fe I lines is considerably T -dependent and parameter solutions from them are vulnerable to slight inadequacies in observational data, while Fe II lines are more robust in this respect. (ii) The number of Fe II lines is by ~ 3 – 4 times as that of Fe I lines, thus the former being expected to yield statistically more reliable results. (iii) A much wider span of χ_{low} is covered by Fe II lines ($0 \lesssim \chi_{\text{low}} \lesssim 13$ eV) than the case of Fe I lines ($0 \lesssim \chi_{\text{low}} \lesssim 5$ eV), which means that the former is definitely more advantageous than the latter for the purpose of T_{eff} determination. Accordingly, the $(T_{\text{eff}}^*, v_t^*)$ results derived from Fe II lines are adopted; i.e., (11150, 0.9) for A, and (10650, 0.1) for B.

Regarding the surface gravity, $\log g = 4.30$ is assumed for both A and B in this study. Although Nordström & Johansen (1994) derived $4.331(\pm 0.025)$ (A) and $4.280(\pm 0.025)$, their conclusion of $\log g_A > \log g_B$ (which is significant in understanding the evolutionary status of this system) appears questionable as discussed in Appendix A. Accordingly, $\log g = 4.30$ was assigned to both A and B with an uncertainty of $\lesssim 0.05$ dex, which is practically sufficient because abundances are less sensitive to this parameter.

As to the model metallicity, solar composition models are adopted, which is a reasonable choice (given that abundances of some elements are sub-solar while those of others are supersolar in chemically peculiar stars) because atmospheric structures of early-type stars do not depend much upon the metallicity (i.e., electrons are donated not by metals but essentially by hydrogen).

The final parameters of AR Aur A and B used for abundance determinations are summarized in Table 2, where probable uncertainties are also given. The Fe abundances (A_i) derived from each of Fe I and Fe II lines corresponding to the adopted Fe II-based T_{eff}^*/v_t^* (11150/0.9 for A and 10650/0.1 for B) are plotted against (W_i) and χ_{low} and the corresponding empirical curves of growth are depicted in the center (Fe I) and right (Fe II) columns of Figure 4 (A) and Figure 5 (B), where

the Fe I results for the unadopted Fe I lines-based parameters are also shown in the left columns for reference. It can be seen from these figures that the required condition (no systematic dependence in A_i upon W_i and χ_{low}) is almost fulfilled.

Table 1: (T_{eff}, v_t) solutions at the minimum of σ .

Lines	T_{eff}^* (K)	v_t^* (km s ⁻¹)	σ^* (dex)	$\langle A \rangle$ (dex)	Fig.
		[AR Aur A]			
Fe I	10927 (397)	1.20 (0.23)	0.102	7.892	3a
Fe II	11172 (187)	0.93 (0.23)	0.143	8.090	3b
		[AR Aur B]			
Fe I	9901 (283)	0.00 (0.17)	0.085	7.301	3c
Fe II	10655 (140)	0.12 (0.19)	0.143	7.790	3d

Columns 2 and 3 give the values of T_{eff} and v_t , at which Fe abundance dispersion is minimized. The corresponding σ and the mean Fe abundance are presented in columns 4 and 5, respectively. See the figures indicated in column 6 for the relevant $\sigma(T_{\text{eff}}, v_t)$ contours. The parenthesized values are the probable uncertainties involved in T_{eff}^* and v_t^* , which were estimated from σ^* by random simulations as described in sect. 3.3 of Takeda (2024a).

Table 2: Adopted atmospheric parameters.

Star	T_{eff} (K)	v_t (km s ⁻¹)	$\log g^{\#}$ (dex)
A	11150 (± 200)	0.9 (± 0.2)	4.30 (± 0.05)
B	10650 (± 150)	0.1 (± 0.2)	4.30 (± 0.05)

Given here are the model atmosphere parameters (based on the solutions obtained from Fe II lines; cf. Table 1) finally adopted for deriving the chemical abundances of AR Aur A and B. The parenthesized values are the estimated typical uncertainties.

[#] g is in cm s⁻².

4 ABUNDANCE DETERMINATION

Based on the model atmospheres with the atmospheric parameters established in Section 3.2, elemental abundances of A and B are determined from the equivalent widths (W_λ) of spectral lines, where W_λ values measured by direct function-

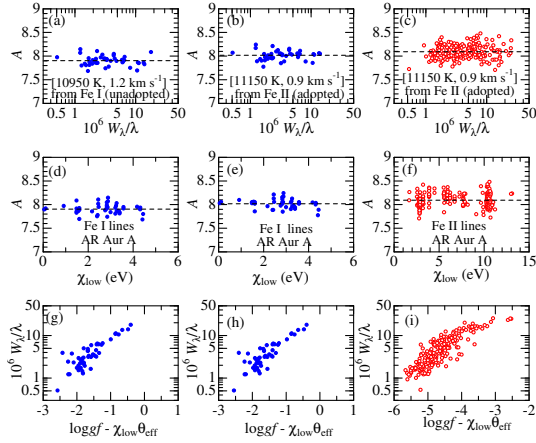


Fig. 4: Fe abundances (A_i) of AR Aur A corresponding to two (T_{eff} , v_t) solutions of minimizing σ , (10950 K, 1.2 km s^{-1} based on Fe I lines though unadopted; left panels) and (11150 K, 0.9 km s^{-1} based on Fe II lines finally adopted; center and right panels), are plotted against equivalent width (W_λ ; top panels) or lower excitation potential (χ_{low} ; middle panels). The mean abundance ($\langle A \rangle$) is also indicated by the horizontal dashed line. In the bottom panels are shown the corresponding empirical curves of growths, where $\log gf - \chi_{\text{low}}(5040/T_{\text{eff}})$ is taken as the abscissa. The results for Fe I and Fe II lines are distinguished by filled blue symbols and open red symbols, respectively.

fitting on the spectrum (cf. Sect. 2.2) are basically employed.

4.1 Spectrum fitting

However, since identification and W_λ measurement done in Section 2.2 was restricted to single-component lines, important multi-component line features (such as He I 4471 or Mg II 4481) could not be included.

Therefore, an alternative synthetic spectrum-fitting approach was additionally applied to selected line features (consisting of single- or multi-components) to evaluate the relevant W_λ inversely from the resulting abundance. Regarding the details of this alternative W_λ -determination approach, section 4 of Takeda et al. (2018) may be consulted.

This synthetic fitting analysis was applied to 12 spectral regions, in order to evaluate the equiv-

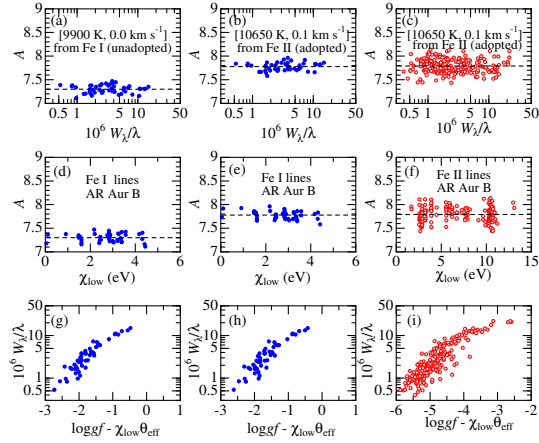


Fig. 5: The results of Fe abundances (A_i) for AR Aur B are presented, corresponding to two (T_{eff} , v_t) solutions of minimizing σ , (9900 K, 0.0 km s^{-1} based on Fe I lines though unadopted; left panels) and (10650 K, 0.1 km s^{-1} based on Fe II lines finally adopted; center and right panels). Otherwise, the same as in Figure 4.

alent widths of 18 line features, as graphically displayed in Figure 6.

4.2 Non-LTE calculations

According to the policy of taking the non-LTE effect into consideration wherever possible, non-LTE abundances were derived for comparatively lighter elements ($Z \leq 15$), for which the author has experiences of non-LTE analysis. Otherwise ($Z \geq 16$), the abundances were derived under the assumption of LTE. The finally adopted (input) abundances in non-LTE calculations (and the related papers) are summarized in Table 3.

Since magnesium (Mg, $Z = 12$) has not been explicitly mentioned in the author's past publications, some explanations are in order. Non-LTE calculations for Mg I and Mg II were conducted for this study by using the non-LTE code described in Takeda (1991). The atomic model was constructed based on Kurucz & Bell's (1995) compilation of atomic data (gf values, levels, etc.), which consists of 108 Mg I terms (up to $19d^3D$ at 61361.5 cm^{-1}) with 771 Mg I radiative transitions and 41 Mg II terms (up to $11g^2G$ at 117639.5 cm^{-1}) with 210 Mg II radiative transitions. Regarding the photoionization rates, the cross-section data taken from TOPbase (Cunto

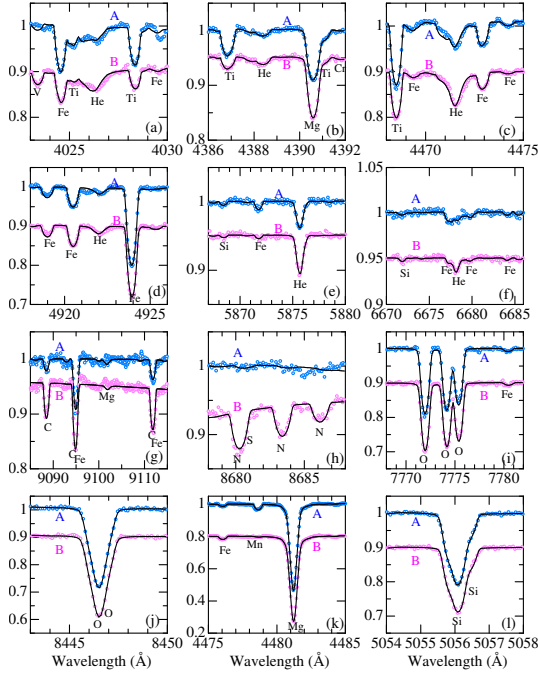


Fig. 6: The accomplished fit of the synthetic spectrum-fitting analysis carried out in 12 regions for the purpose of inverse evaluations of equivalent widths for (a) He I 4026, (b) He I 4388, (c) He I 4471, (d) He I 4922, (e) He I 5876, (f) He I 6678, (g) C I 9089/9095/9112, (h) N I 8680/8683/8686, (i) O I 7772/7774/7775, (j) O I 8446, (k) Mg II 4481, and (l) Si II 5056. The observed and theoretical spectra are depicted by symbols (blue for A, pink for B) and black lines, respectively. As in Figure 2, the scale marked in the ordinate is for A, since the spectra for B are shifted downwards by appropriate amounts (0.05 or 0.1 or 0.2).

& Mendoza 1992) were used for the lower 10 Mg I terms and 12 Mg II terms (while hydrogenic approximation was assumed for all other higher terms). As to the collisional rates, the recipe described in section 3.1.3 of Takeda (1991) was followed.

4.3 Abundance results

After inspection of the list of available lines, it was decided to focus on the following 34 species of 28 elements: He I, C I, N I, O I, Ne I, Na I, Mg I, Mg II, Al I, Al II, Si II, P II, S II, Ar I, Ca I, Ca II,

Table 3: Non-LTE calculations done in this study.

Elem. $Z^{\#}$	$[X/H]_A^*$	$[X/H]_B^*$	References [†]
He 2	-1.0	-0.5	Takeda (1994)
C 6	-0.8	-0.3	Takeda (1992b)
N 7	-0.8	-0.3	Takeda (1992b)
O 8	-0.3	-0.3	Takeda (1992a, 2003)
Ne 10	-1.0	-0.3	Takeda et al. (2010)
Na 11	0.0	0.0	Takeda & Takada-Hidai (1994)
Mg 12	0.0	0.0	this paper (Sect. 4.2)
Al 13	-1.5	+0.2	Takeda (2023)
Si 14	+0.2	+0.2	Takeda (2022)
P 15	+1.0	0.0	Takeda (2024b)

[#] Atomic number.

* Abundances (relative to the solar composition) assigned in non-LTE calculations for each star (in dex), which were (iteratively) chosen so that they may be consistent with the final results of non-LTE abundances.

[†] These papers (and the references quoted therein) may be consulted for more details about the calculations (e.g., adopted model atoms).

Sc II, Ti II, V II, Cr I, Cr II, Mn I, Mn II, Fe I, Fe II, Ni II, Zn I, Sr II, Y II, Zr II, Xe II, Ba II, Ce II, and Nd III. By using the equivalent widths of spectral lines or line features (derived either by direct measurement or synthetic-fitting), the abundances of these elements were determined by using Kurucz’s (1993) WIDTH9 program, which was considerably modified by the author (e.g., treatment of merged multi-component features, taking into account the non-LTE effect, etc.). The resulting detailed line-by-line abundances derived for A and B (and their line-averaged values), along with the observed W_{λ} as well as atomic data of spectral lines, are presented in “abundresults.dat” of online material.

Table 4 presents the mean results averaged over the available lines for each species: $\langle [X/H]_A \rangle$ or $\langle [X/H]_B \rangle$ (mean abundance relative to the Sun; i.e., line-average of $A_i - A_{\odot}$), and $\langle \Delta A_{A-B}^X \rangle$ (mean of line-by-line difference between A and B; i.e., line-average of $A_{i,A} - A_{i,B}$). The reference solar abundances (A_{\odot} ; given in the 3rd column of Table 4)⁴ were taken from Anders and Grevesse (1989) (excepting Fe, for which the value of 7.50 was used), in order to maintain consistency with the author’s previous studies.

⁴ It should be noted that these data may be somewhat outdated as compared to more recent compilations. For example, Asplund et al.’s (2009) solar CNO abundances are by ~ 0.2 – 0.3 dex lower than the values adopted here.

In cases where abundances could not be determined because no lines were measurable, upper-limit abundances were derived by using the following lines: Ne I 6402.248 (1.7), Al I 3944.006 (1.6), Al II 4663.046 (1.4), Ar I 8115.311 (2.9), Sc II 4246.822 (1.5), and Zn I 4722.153 (1.4) for AR Aur A, Mn I 4783.430 (1.5), Xe II 4844.330 (1.5), Ce II 4711.293 (1.5), and Nd III 5127.044 (1.5) for AR Aur B. Here, the values in parentheses are the upper limit equivalent widths (W_{λ}^{ul}) in mÅ estimated by the following relation

$$W_{\lambda}^{\text{ul}} = k \lambda (v_w/c) / (S/N), \quad (1)$$

where $k(= 2)$ is the empirically assigned factor, λ is the wavelength, $v_w(\equiv 1.56 v_e \sin i = 1.56 \times 23) = 36 \text{ km s}^{-1}$ is the full-width at half maximum of the rotational broadening function (in velocity unit), c is the speed of light, and S/N is the signal-to-noise ratio evaluated by the λ -dependent 3rd-order polynomial depicted in Figure 1c and 1d.

As given in “abundresults.dat”, the non-LTE corrections (derived for $Z \leq 15$ elements) are considerably different from line to line. The mean non-LTE abundance corrections averaged over lines ($\langle A_{\text{NLTE}} - A_{\text{LTE}} \rangle$) for A/B are $-0.06 / -0.07$ (He I), $+0.04 / -0.07$ (C I), $-0.21 / -0.44$ (N I), $-0.49 / -0.47$ (O I), $\dots / -0.07$ (Ne I), $-0.26 / -0.32$ (Na I), $+0.03 / +0.01$ (Mg I), $-0.04 / -0.04$ (Mg II), $\dots / +0.35$ (Al I), $\dots / -0.01$ (Al II), $-0.03 / -0.02$ (Si II), $-0.10 / -0.24$ (P II). Regarding the abundances derived for other $Z > 15$ species, for which LTE was assumed in this study, little can be said about their non-LTE effects. We may speculate, however, that the abundances of some elements (e.g., Ca, Sr, Zr, Ba) may suffer appreciable non-LTE corrections (as much as several tenths dex) by consulting the recent work of Mashonkina et al. (2020), who studied the non-LTE effects in deriving the abundances of 14 elements (from He to Nd) for nine A- and B-type stars.

The sensitivities of abundance results to changing the atmospheric parameters (T_{eff} , v_t , and $\log g$) are also presented in Table 4, where we can see from this table that the impact of T_{eff} is more appreciable than the other two. That is, abundance errors due to typical uncertainties in T_{eff} ($\sim \pm 200 \text{ K}$; cf. Table 2) are $\lesssim 0.1\text{--}0.2$ dex, while those due to v_t ($\pm 0.2 \text{ km s}^{-1}$) as well as $\log g$ (± 0.05 dex) are only a few hundredths dex in most cases (note that the Δ^{Tvg} values given in Table 4 correspond to perturbations of T_{eff} by 250 K, v_t

by 0.4 km s^{-1} , and $\log g$ by 0.1 dex; i.e., twice as large as the typical ambiguities for the latter two).

5 DISCUSSION

5.1 T_{eff} and v_t for A and B

The values of T_{eff} and v_t were established by using Fe II lines in this study (Sect. 3). Comparing these spectroscopic $T_{\text{eff,A}}/T_{\text{eff,B}}$ (11150/10650 K) with Nordström & Johansen’s (1994) photometric SED-based determinations (10950/10350 K), we can see that, while our results tend to be somewhat higher than theirs by $\sim 200\text{--}300 \text{ K}$ in the absolute scale, the relative differences between A and B ($\Delta T_{\text{eff,A-B}} = +500 \text{ K}$ in this study and $+600 \text{ K}$ in their paper) are reasonably consistent with each other.

Regarding v_t , for which determinations for this AR Aur system have failed so far, the results (0.9 km s^{-1} for A and 0.1 km s^{-1} for B) concluded by the analysis of Fe II lines in Section 3 may be regarded as significant. It should be noted that similar inequality relation of $v_{t,A} > v_{t,B}$ (i.e., larger v_t for higher T_{eff}) was obtained also from Fe I lines (though not adopted; cf. Table 1). Therefore, this increase of v_t with T_{eff} in AR Aur A and B (late B-type stars) does not follow the trend seen in early A-type stars where v_t tends to progressively decrease with T_{eff} (see, e.g., Takeda et al. 2008). This characteristics of appreciably smaller v_t values ($\sim 0\text{--}1 \text{ km s}^{-1}$) in late-B dwarfs (in comparison with early-A dwarfs which have typical v_t of $\sim 2 \text{ km s}^{-1}$) is consistent with the results of several spectroscopic studies done by other investigators (e.g., Allen 1998; Hubrig et al. 1999; Saffe et al. 2011).⁵ Considering that A and B are quite similar in terms of other parameters, this fact of discrepant v_t under only a small difference in T_{eff} might be a clue to understand the nature of micro-turbulence in late B-type stars.

⁵ The literature v_t values of late-B type stars compiled by Sadakane (1990; cf. table 4 therein) are as large as $\sim 1\text{--}2 \text{ km s}^{-1}$ with a roughly decreasing tendency with T_{eff} (similarly to the case of early A-type stars), which may appear to contradict the trend mentioned here. Note, however, since class V (dwarfs), class IV (subgiants), and class III (giants) are mixed in Sadakane’s (1990) sample, any definite conclusion can not be made from such an inhomogeneous data set.

Table 4: Results of elemental abundances for AR Aur A and B.

Z	Species	A_{\odot}	N	$\langle[X]_A\rangle$	N_A	$\langle[X]_B\rangle$	N_B	$\langle\Delta A_{A-B}^X\rangle$	N_{A-B}	Δ_A^{T-}	Δ_B^{T+}	Δ_A^{v-}	Δ_B^{v+}	Δ_A^{g+}	Δ_B^{g+}
(1)	(2)	(3)	(4)	(5)	(6)	(7)	(8)	(9)	(10)	(11)	(12)	(13)	(14)	(15)	(16)
(non-LTE analysis)															
2	He I	11.00	6	-1.12	(6)	-0.55	(6)	-0.57	(6)	+14	-15	+02	-01	+06	+06
6	C I	8.56	7	-0.78	(4)	-0.37	(7)	-0.34	(4)	-09	+10	-00	+00	-02	-02
7	N I	8.05	11	-1.68	(3)	-0.54	(10)	-1.17	(3)	-04	+03	-03	+00	+00	+00
8	O I	8.93	9	-0.36	(9)	-0.37	(9)	-0.03	(8)	-02	+01	-00	+00	-00	-00
10	Ne I	8.09	1	< -0.8	(0)	-0.29	(1)	< -0.5	(0)	...	-13	...	+01	...	+05
11	Na I	6.33	4	-0.08	(4)	+0.02	(4)	-0.11	(4)	-10	+12	-01	-00	-02	-03
12	Mg I	7.58	7	+0.09	(6)	+0.15	(5)	-0.06	(6)	-14	+14	+01	-01	-04	-04
12	Mg II	7.58	8	-0.09	(8)	-0.02	(8)	-0.07	(8)	+01	-00	+01	-01	+00	-00
13	Al I	6.47	2	< -1.3	(0)	+0.28	(2)	< -1.7	(0)	...	+13	...	-01	...	-00
13	Al II	6.47	6	< -1.5	(0)	+0.16	(6)	< -1.7	(0)	...	-07	...	+01	...	+03
14	Si II	7.55	9	+0.20	(9)	+0.07	(7)	+0.07	(7)	+04	-04	+02	-01	+03	+03
15	P II	5.45	5	+1.26	(5)	+0.12	(1)	+0.97	(1)	+07	-07	-00	+00	+04	+04
(LTE analysis)															
16	S II	7.21	2	-0.29	(2)	-0.02	(2)	-0.27	(2)	+10	-11	+00	-00	+06	+06
18	Ar I	6.56	2	< -0.3	(0)	+0.37	(2)	< -0.5	(0)	...	+01	...	+01	...	+00
20	Ca I	6.36	1	-0.27	(1)	-0.22	(1)	-0.05	(1)	-24	+25	+00	-00	-07	-07
20	Ca II	6.36	7	-0.20	(6)	-0.32	(6)	+0.18	(6)	-10	+11	+01	-01	-02	-02
21	Sc II	3.10	1	< -1.4	(0)	-0.72	(1)	< -0.7	(0)	...	+14	...	-00	...	-00
22	Ti II	4.99	59	+0.69	(50)	+0.08	(42)	+0.62	(39)	-10	+10	+04	-01	+01	+01
23	V II	4.00	4	+0.25	(1)	+0.39	(4)	-0.09	(1)	-07	+07	+01	-01	+02	+02
24	Cr I	5.67	3	+0.65	(2)	+0.43	(2)	+0.01	(1)	-16	+17	+01	-00	-03	-03
24	Cr II	5.67	47	+0.50	(35)	+0.39	(41)	+0.12	(31)	-04	+04	+03	-01	+03	+03
25	Mn I	5.39	2	+1.25	(2)	< +0.2	(0)	> +1.1	(0)	-15	...	+00	...	-03	...
25	Mn II	5.39	38	+1.31	(33)	+0.39	(7)	+0.95	(6)	-02	+03	+02	-00	+03	+03
26	Fe I	7.50	101	+0.56	(60)	+0.31	(88)	+0.26	(46)	-13	+14	+02	-01	-03	-03
26	Fe II	7.50	339	+0.62	(304)	+0.30	(240)	+0.31	(211)	+01	-01	+03	-01	+03	+03
28	Ni II	6.25	7	-0.79	(1)	+0.62	(7)	-1.39	(1)	-01	-01	+01	-01	+04	+03
30	Zn I	4.60	1	< +0.5	(0)	+0.78	(1)	< -0.3	(0)	...	+12	...	-00	...	-03
38	Sr II	2.90	2	+1.81	(2)	+0.89	(2)	+0.92	(2)	-17	+18	+23	-11	-02	-03
39	Y II	2.24	11	+2.37	(11)	+0.75	(1)	+1.45	(1)	-16	+16	+09	-00	-01	-01
40	Zr II	2.60	9	+1.67	(7)	+0.77	(3)	+0.91	(3)	-13	+13	+04	-01	+00	+01
54	Xe II	2.23	1	+4.70	(1)	< +3.9	(0)	> +0.8	(0)	+11	...	+04	...	+09	...
56	Ba II	2.13	3	+1.03	(2)	+1.56	(2)	-0.65	(1)	-16	+18	+02	-07	-02	-03
58	Ce II	1.55	1	+5.01	(1)	< +3.9	(0)	> +1.1	(0)	-14	...	+01	...	-02	...
60	Nd III	1.50	12	+2.51	(10)	< +0.7	(0)	> +1.9	(0)	-04	...	+04	...	+04	...

(1) Atomic number. (2) Element species. (3) Reference solar abundances (in the usual normalization of $H = 12.00$), which are taken from Anders & Grevesse's (1989) compilation (except for Fe, for which 7.50 is adopted). (4) Number of lines adopted for this species. (5) Mean of $[X/H]_A$ (relative abundance for A in comparison with the Sun) averaged over lines. (6) Actual number of lines used for deriving $\langle[X/H]_A\rangle$. (7) Mean of $[X/H]_B$. (8) Actual number of lines employed for $\langle[X/H]_B\rangle$. (9) Mean of ΔA_{A-B}^X (differential line-by-line abundance between A and B) averaged over lines. (10) Actual number of lines used for calculating $\langle\Delta A_{A-B}^X\rangle$. (11) Abundance change for A in response to $\Delta T_{\text{eff}} = -250$ K. (12) Abundance change for B in response to $\Delta T_{\text{eff}} = +250$ K. (13) Abundance change for A in response to $\Delta v_t = -0.4$ km s $^{-1}$. (14) Abundance change for B in response to $\Delta v_t = +0.4$ km s $^{-1}$. (15) Abundance change for A in response to $\Delta \log g = +0.1$ dex. (16) Abundance change for B in response to $\Delta \log g = +0.1$ dex.

All abundance-related data (A_{\odot} , $\langle[X/H]\rangle$, Δ) are in unit of dex. See Section 4.3 regarding how the upper limit abundance was estimated for unmeasurable cases. Note that only the 1st and 2nd decimals are shown in the data of (11)–(16) (i.e., they should be divided by 100).

5.2 Trends of chemical abundances

Based on the results in Table 4, $\langle[X/H]_A\rangle$, $\langle[X/H]_B\rangle$, and $\langle\Delta A_{A-B}^X\rangle$ are plotted against Z in Figure 7a, 7b, and 7c. Considering the impact of uncertainties in atmospheric parameters (cf.

Table 2 and Table 4) and the size of standard deviations in the averages (cf. “abundresults.dat”), typical statistical errors involved with the data symbols in Figure 7 may be estimated as $\pm \lesssim 0.1$ – 0.2 dex. It should be kept mind, however, that additional systematic errors might be possible in $[X/H]$ val-

ues related to other factors (e.g., reference solar abundances, gf values, non-LTE effect for $Z > 15$ elements, etc.), while ΔA_{A-B}^X values (line-by-line differential abundances) are distinctly more advantageous because they are almost irrelevant to such systematic error sources.

Several notable characteristics are observed by inspecting Figure 7, as summarized below (the symbols “/” and “\”) to indicate average values are omitted for simplicity):

- Roughly speaking, $[X/H]$ (departure from the solar composition) tends to increase with Z in the global sense for both A and B (Fig. 7a and 7b); i.e., $[X/H] < 0$ at $Z \lesssim 10$, $[X/H] \sim 0$ at $10 \lesssim Z \lesssim 20$, and $[X/H] > 0$ at $Z \gtrsim 20$. Quantitatively, the degree of Z -dependence (or the slope of linear-regression line) is steeper for A than for B. As a result, ΔA_{A-B}^X also shows a similar Z -dependent trend (Fig. 7c)
- Yet, the dispersion of $[X/H]_A$ is considerably large, because some elements show conspicuous deviations from the global trend by as much as $\sim \pm 1$ dex; that is, the pronounced deficits of N, Al, Sc, and Ni; or the prominent excesses of P and Mn (and rare earths). Since these are the characteristics of chemically peculiar stars of HgMn type (e.g., Ghazaryan & Alecian 2016), we can state that AR Aur A is surely a HgMn star.
- In contrast, the Z -dependence of $[X/H]_B$ is apparently more tight, which almost linearly correlate with Z ($[X/H]_B \simeq -0.6 + 0.04Z$) as depicted in Figure 7b. Actually, it is only Sc and high- Z elements (Xe, Ce, Nd) that markedly deviate from this relation. Folsom et al. (2010) suggested AR Aur B to belong to a weak Am star. Admittedly, the “global” trend of its abundance pattern is similar to that shown by Am-Fm stars (see, e.g., fig. 5 in Smith 1996). However, on a close inspection, the abundance peculiarities of Am stars do not exhibit such a remarkable Z -dependent near-linearity. For example, $[X/H]$ values of Sirius (well-known hot Am star) show appreciable local fluctuations (cf. fig. 4 in Michaud et al. 2011), though surely tending to increase with Z in the global sense. Therefore, a new type specific to late B-type stars (Bm stars?) might as well be assigned to this kind of peculiarity in AR Aur B.

5.3 Comparison with previous results

Let us compare the abundance characteristics of AR Aur A and B resulting from this investigation (Sect. 5.2) with those reported by previous chemical abundance studies for this system (Sect. 1).

Khokhlova et al.’s (1995) work was the first attempt to determine the abundances of A and B for various elements. Although high precision would not have been expected because of methodological disadvantages in comparison with the present-day standard (i.e., use of photographic spectrogram, difficulty in measuring W_λ on double-lined spectra, classical curve-of-growth analysis), their conclusions are qualitatively consistent with our results (typical HgMn-type peculiarity in A, less pronounced anomalies of different kind in B). The same applies also to Ryabchikova’s (1998) results of reanalyzing Khokhlova et al.’s W_λ data using model atmospheres. Folsom et al. (2010; sect. 5 therein) stated that the abundances obtained by them are in reasonable agreement with those of Ryabchikova (1998), except that their results are appreciably lower than the latter in some specific elements (C, Mn, Sr, Y, and Pt for A; Ti, Mn, Fe, and Ba for B).

The elemental abundances of AR Aur A and B determined by Folsom et al. (2010) based on the spectrum synthesis technique are more extensive and probably more reliable than any other previous determinations. Therefore, their $[X/H]_A$ and $[X/H]_B$ values (taken from table 3 therein) are overplotted in Figure 7 for comparison. As seen from this figure, their results (light-green crosses) are satisfactorily consistent with those of this study (black bullets), though some minor discrepancies are observed in several elements (such as He, C, O, Sr, Y, Zr, and Ba). This may be attributed to several factors (e.g., non-LTE effect, different choice of fiducial solar abundance, difference in the adopted microturbulence).

Although the main purpose of Paper I was to establish the abundances of C, N, and O for both of the binary components, those of Na, Si, Ca, Ti, Fe, and Ba (obtained as by-products) were also presented. Those $[X/H]$ values (cf. table 7 therein) determined for AR Aur A and B do not necessarily agree well with the present results. This is because (i) there were some cases where the lines used in Paper I (primary attention being paid to A-type stars) were too weak for late B-type stars, and (ii) microturbulences ($v_{t,A}, v_{t,B}$) of (1.0, 1.6 km s⁻¹)

employed in Paper I were different from the values ($0.9, 0.1 \text{ km s}^{-1}$) adopted in this paper (especially for B). As such, considerable discrepancies (larger than 0.3 dex) are seen in $[C/H]_A$, $[C/H]_B$, $[Na/H]_A$, $[Si/H]_B$, $[Ca/H]_A$, $[Ba/H]_A$, and $[Ba/H]_B$. In any case, the abundances of AR Aur derived in Paper I should be replaced by the new results of this investigation presented in Table 4.

5.4 Origin of compositional differences between A and B

Now that the nature of surface abundances for AR Aur A and B has been elucidated, the key issue to be considered is “what is the cause of such appreciable chemical differences between these two similar stars?”

Whereas the chemical aberrations of component B ($T_{\text{eff}} = 10650 \text{ K}$) are rather weak and organized ($[X/H]$ is almost linearly dependent upon Z), the slightly hotter A ($T_{\text{eff}} = 11150 \text{ K}$) in turn exhibits wildly conspicuous HgMn-type abundance anomalies (strong deficit of N, Al, Sc, Ni; prominent excess of P, Mn). Which physical process is responsible for this remarkable transmutation of surface chemistry for only a small ($\sim 500 \text{ K}$) change in T_{eff} ?

If this transition is caused by the difference of T_{eff} , HgMn peculiarity must be a very T_{eff} -sensitive phenomenon in the sense that it is suddenly triggered once T_{eff} exceeds a critical value at $\simeq 11000 \text{ K}$. Admittedly, the existence of such a T_{eff} limit is consistent with the statistical study of late B-type stars by Wolff & Preston (1978), who found that HgMn stars are observed only at $11000 \text{ K} \lesssim T_{\text{eff}} \lesssim 16000 \text{ K}$. Yet, it may still be wondered which kind of mechanism is underlying in such abrupt surface abundance changes at this critical T_{eff} .

We should recall that v_t is appreciably discordant between A (0.9 km s^{-1}) and B (0.1 km s^{-1}). One may question whether this difference has something to do with the distinction of abundance characteristics between A and B. However, if more stable atmosphere is favored for the emergence of chemical peculiarity (as often postulated in element diffusion theory), this inequality in v_t (i.e., stronger anomaly for larger turbulence) may be contradictory to our intuitive picture.

Another issue worth consideration is the evolutionary status of the AR Aur system. Nordström & Johansen (1994) concluded from the unusual in-

equality of radii ($R_B > R_A$) despite of the mass difference ($M_B < M_A$) that B is likely to be still in the pre-main sequence stage of contraction phase, while A is already on the main sequence of hydrogen burning phase. However, their conclusion is unconvincing and questionable, as separately discussed in Appendix A. But, if this scenario is really the case, such a difference in the evolutionary phase may affect the surface chemistry. For example, strong abundance anomaly would take place quickly after a star has arrived at the main sequence where atmospheric stability is realized (corresponding to A), while conspicuous chemical peculiarity would be difficult to develop during the unstable contraction phase (corresponding to B).

In any event, the abundance characteristics of AR Aur A and B (especially their marked differences from each other) established in this investigation may serve as important observational facts for any theory trying to explain the chemical anomaly of late B-type stars.

6 SUMMARY AND CONCLUSION

The close binary system AR Aur A+B is of astrophysical importance, because surface compositions of both are known to exhibit appreciable differences despite that they are similar B9V and B9.5V main-sequence stars. By investigating the chemical abundances characteristics of A and B along with the differences of stellar atmospheric parameters, we may gain useful physical insight into the mechanism of how and which chemical anomaly takes place in late B-type stars.

Although stellar parameters of this system are comparatively well established by making use of the merit of spectroscopic/eclipsing binary, reliable spectroscopic determinations of T_{eff} and v_t (important atmospheric parameters for spectroscopic analysis) have not yet been done. Likewise, publications of extensive elemental abundance study for both A and B based on high-quality data are still insufficient, reflecting the difficulty of analyzing complex double-lined spectra of AR Aur.

Motivated by this situation, the author decided to carry out a detailed spectroscopic study for each component, in order to determine the key atmospheric parameters and elemental abundances of A and B as precisely as possible and to examine how they compare with each other.

Regarding the basic observational material, the spectrum-disentangle technique was applied to

a set of original double-line spectra taken at different orbital phases to obtain the decomposed spectra of A and B. Based on these disentangled spectra (covering 3900–9200 Å), many lines judged to be usable were identified and their W_λ were measured by the direct function-fitting. In addition, W_λ values of important line features (even if they consist of complex multi-components) were evaluated by applying the spectrum-synthesis technique.

The values of (T_{eff}, v_t) were determined from Fe II lines by requiring that abundances do not show any systematic dependence upon W_λ and χ_{low} , which turned out (11150 K, 0.9 km s⁻¹) and (10650 K, 0.1 km s⁻¹) for A and B, respectively.

The chemical abundances of 28 elements (34 species) were derived from the W_λ values of many lines, where the non-LTE effect was taken into account for comparatively lighter elements of $Z \leq 15$. The following characteristics were found in the resulting $[X/H]_A$ and $[X/H]_B$.

–(1) Qualitatively, a rough Z -dependent tendency holds for both A and B that light elements ($Z \lesssim 10$ such as He, C, N, O) are underabundant, heavier elements ($Z \gtrsim 20$; such as Fe group, s-process, rare earths) overabundant, and nearly solar for intermediate cases ($10 \lesssim Z \lesssim 20$). Likewise, a similar trend of increasing with Z is roughly seen in the differential abundances between A and B (ΔA_{A-B}^X), since the peculiarity is quantitatively more conspicuous in A than in B.

–(2) Yet, regarding the hotter A, several elements show strikingly large peculiarities (e.g., very deficient N, Al, Sc, Ni or very overabundant P, Mn; leading to a considerable dispersion). These are the well-known characteristics of HgMn stars.

–(3) In contrast, the situation in the cooler B is apparently more simple in the sense that the progressive Z -dependence of $[X/H]_B$ almost follows the linear relation ($[X/H]_B = -0.6 + 0.04Z$) with only a small dispersion. Therefore, B shows a comparatively weak and rather organized peculiarity.

Therefore, the next important task would be to clarify the cause why such remarkably dissimilar type of chemical peculiarities are observed in these two similar late B-type stars (with a small T_{eff} difference of ~ 500 K), for which further contributions of theoreticians are awaited.

Acknowledgements Data analysis (numerical calculation of spectrum disentangling) was carried out on the Multi-wavelength Data Analysis

System operated by the Astronomy Data Center (ADC), National Astronomical Observatory of Japan. This investigation has made use the VALD database operated at Uppsala University, the Institute of Astronomy RAS in Moscow, and the University of Vienna.

ONLINE MATERIALS

This article accompanies the following online materials (electronic data files). See “ReadMe” for the details about their contents.

- ReadMe
- spectra_A.txt
- spectra_B.txt
- identlist_A.dat
- identlist_B.dat
- abundresults.dat

References

- Allen, C. S. 1998, Abundance analysis of normal and mercury-manganese type late-B stars from optical spectra (PhD Thesis: University College London) [<https://discovery.ucl.ac.uk/id/eprint/10097529/>]
- Anders, E., & Grevesse, N. 1989, *Geochim. Cosmochim. Acta*, 53, 197
- Asplund, M., Grevesse, N., Sauval, A. J., & Scott, P. 2009, *ARA&A*, 47, 481
- Bressan, A., Marigo, P., Girardi, L., et al. 2012, *MNRAS*, 427, 127
- Cunto, W., & Mendoza C. 1992, *Rev. Mex. Astron. Astrofis.*, 23, 107
- Folsom, C.P., Kochukhov, O., Wade, G.A., Silvester, J., & Bagnulo, S. 2010, *MNRAS*, 407, 2383
- Ghazaryan, S., & Alecian, G. 2016, *MNRAS*, 460, 1922
- Hubrig, S., Castelli, F., & Mathys, G. 1999, *A&A*, 341, 190
- Khokhlova, V.L., Zverko, Yu., Zhizhnovskii, I., & Griffin, R.E.M. 1995, *Astron. Lett.*, 21, 818
- Kurucz, R.L. 1993, Kurucz CD-ROM, No. 13 (Harvard-Smithsonian Center for Astrophysics)
- Kurucz, R.L., & Bell, B. 1995, Kurucz CD-ROM, No. 23 (Harvard-Smithsonian Center for Astrophysics)
- Mashonkina, L., Ryabchikova, T., Alexeeva, S., Sitnova, T., & Zatsarinny, O. 2020, *MNRAS*, 499, 37
- Michaud, G., Richer, J., & Vick, M. 2011, *A&A*, 534, A18

- Nordström, B., & Johansen, K.T. 1994, *A&A*, 282, 787
- Ryabchikova, T. 1998, *Contrib. Astron. Obs. Skalnaté Pleso*, 27, 319
- Ryabchikova, T., Piskunov, N., Kurucz, R.L., et al. 2015, *Phys. Scr.*, 90, 054005
- Sadakane, K. 1990, in *Lecture Note in Physics*, 357, Accuracy of element abundances from stellar atmospheres (Berlin: Springer), p.57
- Saffe, C., Núñez, N., & Levato, H. 2011, *RMxAA*, 47, 219
- Smith, K.C. 1996, *Ap&SS*, 237, 77
- Takeda, Y. 1991, *A&A*, 242, 455
- Takeda, Y. 1992a, *PASJ*, 44, 309
- Takeda, Y. 1992b, *PASJ*, 44, 649
- Takeda, Y. 1994, *PASJ*, 46, 181
- Takeda, Y. 2003, *A&A*, 402, 343
- Takeda, Y. 2022, *Contrib. Astron. Obs. Skalnaté Pleso*, 52, 5
- Takeda, Y. 2023, *Contrib. Astron. Obs. Skalnaté Pleso*, 53, 31
- Takeda, Y. 2024a, *Astron. Nachr.*, 345, e20230174
- Takeda, Y. 2024b, *Acta Astron.*, 74, 43
- Takeda, Y., Han, I., Kang, D.-I., Lee, B.-C., & Kim, K.-M. 2008, *JKAS*, 41, 83
- Takeda, Y., Han, I., Kang, D.-I., Lee, B.-C., & Kim, K.-M. 2019, *MNRAS*, 485, 1067 (Paper I)
- Takeda, Y., Kambe, E., Sadakane, K., & Masuda, S. 2010, *PASJ*, 62, 1239
- Takeda, Y., Kawanomoto, S., Ohishi, N., et al. 2018, *PASJ*, 70, 91
- Takeda, Y., & Takada-Hidai, M. 1994, *PASJ*, 46, 395
- Takeda, Y., Takada, M., & Kitamura, M. 1979, *PASJ*, 31, 821
- Wolff, S.C., & Wolff, R.J. 1976, in *Physics of Ap Stars*, IAU Colloquium No.32, ed. W.W. Weiss, H. Jenkner, and H.J. Wood (Universitätssternwarte Wien, Vienna), p.503
- Wolff, S.C., & Preston, G.W. 1978, *ApJS*, 37, 371
- Zverko, J., Žižňovský, J., & Khokhlova, V.L. 1997, *Contrib. Astron. Obs. Skalnaté Pleso*, 27, 41

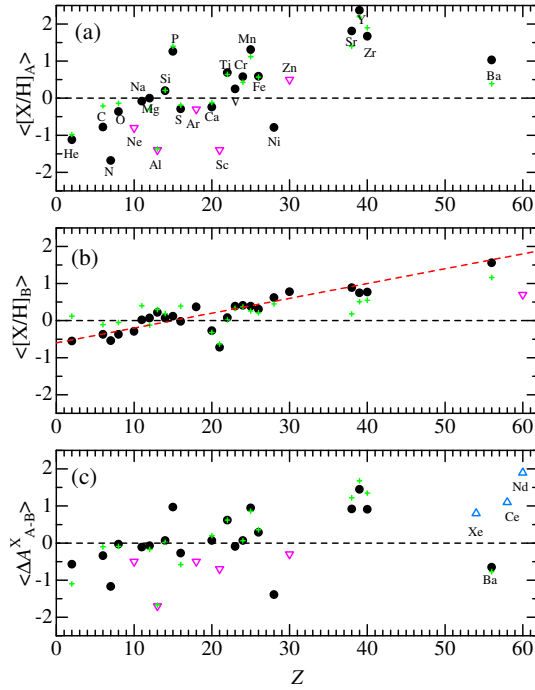


Fig. 7: Plotted against Z (atomic number) in black filled bullets are (a) $\langle [X/H]_A \rangle$ (averaged differential abundance of element X relative to the Sun for AR Aur A), (b) $\langle [X/H]_B \rangle$ (ditto for AR Aur B), and (c) $\langle \Delta A_{A-B}^X \rangle$ (averaged line-by-line differential abundance of element X between A and B), for 28 elements (He, C, N, O, Ne, Na, Mg, Al, Si, P, S, Ar, Ca, Sc, Ti, V, Cr, Mn, Fe, Ni, Zn, Sr, Y, Zr, Xe, Ba, Ce, and Nd) based on the data in Table 4. Regarding the elements where two results of different ionization stages are available (Mg, Al, Ca, Mn, Fe), their mean values are adopted here (exceptionally, the result for Mn II is used for Mn because that for Mn I is only the upper limit). The upper limit and lower limit values are indicated by pink open inverse triangles and blue open normal triangles, respectively. In panel (b), the linear relation, $\langle [X/H]_B \rangle = -0.6 + 0.04Z$, is depicted by a dashed line. Note that in panels (a) and (b), some results for high- Z elements (Xe, Ce, Nd) are outside of the plot range. For reference, Folsom et al.'s (2010) results of $[X/H]_A$, $[X/H]_B$, and $[X/H]_A - [X/H]_B$ are also shown by light-green small crosses in each of the panels.

Appendix A: IS AR AUR B IN PRE-MAIN SEQUENCE STAGE?

Nordström & Johansen (1994) concluded that AR Aur B is still in the contracting phase of pre-main-sequence, whereas AR Aur A is already in the H-burning phase on the main sequence. This conclusion is based on the radius ratio they derived for this system $R_B/R_A = 1.02 \pm 0.015 (> 1)$. That is, since the mass ratio is robustly determined from the spectroscopic orbital elements as $M_B/M_A = 2.29/2.48 = 0.925 (< 1)$, such an inequality relation ($R_B/R_A > 1$) is impossible if both A and B are main-sequence stars (where R increases with M). Thus, the only solution simultaneously satisfying both conditions in terms of R and M is to regard that B has not yet reached the main sequence but A is already on it.

However, their argument is not convincing. Since precisely determining R_B/R_A from light curve analysis is difficult for the case of AR Aur (partially eclipsing system with nearly similar components), they invoked the observed equivalent width ratio (W_B/W_A) of the strong Mg II 4481 line by making use of the relation

$$\begin{aligned} W_B^{\text{obs}}/W_A^{\text{obs}} &= (W_B^{\text{int}}/W_A^{\text{int}})(L_B/L_A) \\ &= (W_B^{\text{int}}/W_A^{\text{int}})(J_B/J_A)(R_B/R_A)^2, \end{aligned} \quad (\text{A.1})$$

where W^{obs} and W^{int} are the observed equivalent width on the double-line spectrum and the intrinsic equivalent width ($W^{\text{obs}} < W^{\text{int}}$ because of the dilution effect), while J and L are the surface brightness and the luminosity at the waveband of the line. That is, since $W_B^{\text{obs}}/W_A^{\text{obs}}$ is directly measurable by spectroscopic observations and J_B/J_A is derived from photometric solutions, R_B/R_A can be determined from Equation (A.1) if $W_B^{\text{int}}/W_A^{\text{int}}$ is somehow known.

The serious weak point of this method is the necessity of ‘‘assuming’’ some appropriate value for $W_A^{\text{int}}/W_B^{\text{int}}$, because it is unknowable in advance. Nordström & Johansen (1994) adopted $W_A^{\text{int}}/W_B^{\text{int}} = 0.925 \pm 0.005$ (or $W_B^{\text{int}}/W_A^{\text{int}} = 1.081 \pm 0.006$) based on the rough linear relation between W_{4481}^{int} and the surface flux (dependent upon the spectral type or T_{eff}) constructed from the data of several late B-type stars (cf. their fig. 10). In other words, they considered only the difference of T_{eff} between two components, but assumed other parameters affecting the strength of

Mg II 4481 line to be the same. This is unjustifiable because a slight difference in Mg abundances and a large discordance in v_t actually exist between A and B (as clarified in this study). As such, their assumed $W_B^{\text{int}}/W_A^{\text{int}}$ ratio must suffer appreciable systematic errors due to other factors neglected by them (declared uncertainty of only 0.5% is too optimistic). Accordingly, their final result of $R_B/R_A = 1.02 \pm 0.015$ is not trustworthy, because actual error would be more significant (this error of 1.5% is nothing but due to the uncertainty involved in their $W_B^{\text{obs}}/W_A^{\text{obs}}$).

It should also be pointed out that, although both components being in different evolutionary stages (A: main sequence, B: pre-main sequence) may be conceptually possible, it must be a rare incidence (even in such a circumstance) to observe them as almost similar stars ($M_A \simeq M_B$ and $R_A \simeq R_B$) because evolutionary time scales are markedly different. Figure A.1 illustrates how the physical parameters (T_{eff} , L , R , and $\log g$) of 2.1, 2.2, 2.3, 2.4, 2.5, 2.6, 2.7, and 2.8 M_{\odot} stars vary in the pre-main-sequence phase ($t < 0$) and in the main-sequence phase ($t \geq 0$), which are taken from Bressan et al.’s (2012) theoretical stellar evolution calculations. It can be easily seen from this figure that the time scale of parameter variations due to evolution is much shorter at $t < 0$ than that at $t \geq 0$. Admittedly, if the timing of star formation for A and B is slightly different and the condition of $t_B < 0 < t_A$ is appropriately satisfied, it may be possible to observe $R_B > R_A$ simultaneously with $M_B < M_A$ (cf. Figure A.1c). Yet, in order to realize the near-similarity of R in this case, t_A and (especially) t_B have to be at the pinpointed timing, which would rarely happen by coincidence. In short, AR Aur A and B are too similar to regard B as being still in the pre-main-sequence phase.

Although the argument of Nordström & Johansen (1994) seems to be questionable as described above, it is premature to conclude that it is incorrect. This possibility should still be further investigated. We should note that Folsom et al. (2010) independently carried out a similar analysis using the Mg II 4481 line and obtained the radius ratio $R_B/R_A = 1.033 \pm 0.005$ (confirming the inequality $R_B/R_A > 1$ with even higher precision) which is in support of Nordström & Johansen’s (1994) consequence. Unfortunately, since any detailed account is not given regarding how they derived this value (i.e., adopted $W_B^{\text{obs}}/W_A^{\text{obs}}$ or

$W_B^{\text{int}}/W_A^{\text{int}}$, evaluation of errors, etc.), it is hardly possible to comment on their result.

In any case, given that this is a difficult problem demanding to detect only a slight difference of R with high precision, it is not sufficient to invoke only one Mg II 4481 line to draw any definite conclusion. Such an analysis should be done for at least several lines, in order to confirm whether similar results are derived from different lines.

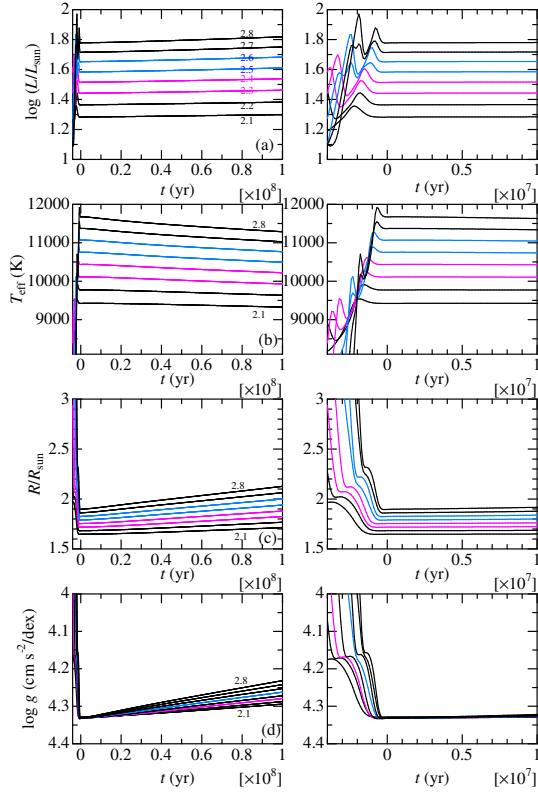


Fig. A.1: Evolution of physical parameters of main-sequence stars (metallicity $Z = 0.02$) with the masses of 2.1, 2.2, 2.3, 2.4, 2.5, 2.6, 2.7, and $2.8 M_{\odot}$, based on Bressan et al.'s (2012) PARSEC database. Plotted against the elapsed time (t) are (a) L (bolometric luminosity), (b) T_{eff} (effective temperature), (c) R (radius), and (d) $\log g$ (surface gravity). Note that the origin ($t = 0$) corresponds to the beginning of H burning in the core (Zero-Age Main Sequence). The left and right panels are paired and different only in the covered time span; the former (global view) is from -4×10^6 yr to $+1 \times 10^8$ yr, while the latter (magnified view) is from -4×10^6 yr to $+1 \times 10^7$ yr. The results for the mass values almost corresponding to AR Aur A and B ($2.5\text{--}2.6 M_{\odot}$ for A, $2.3\text{--}2.4 M_{\odot}$ for B) are colored in blue and pink, respectively. Since the results for 2.5 and $2.7 M_{\odot}$ are not available in the original data, those of $2.4/2.6 M_{\odot}$ and $2.6/2.8 M_{\odot}$ were simply averaged, respectively.